Textures and Microstructures, 1988, Vols. 8 & 9, pp. 639–678
Reprints available directly from the publisher
Photocopying permitted by license only

Printed in the United Kingdom

Texture and Lattice Deformation Pole Figures of Machined Surfaces

G. MAURER, H. NEFF, B. SCHOLTES and E. MACHERAUCH
Institut für Werkstoffkunde I, Universität Karlsruhe, FRG.

(Received 6 September 1987; in final form 25 September 1987)

Dedicated to the memory of Professor Günter Wassermann

A short review of the current knowledge about machining induced texture states is given. The applied methods for the determination of texture and residual stress states are outlined. The surface textures and residual stress states present after grinding, milling and shot peening of initially residual stress- and texture-free as well as of 78% cold-rolled plain carbon steel are presented. Texture and residual stress states are represented by texture and lattice deformation pole figures. In the initially texture-free specimens, machining by grinding and milling gives rise to weak, but typical asymmetric textures. The appertaining principal residual stress systems do not coincide with the specimen system. Shot peening causes a centrosymmetric texture and residal stress state. The cold-rolling texture and residual stress state is significantly changed due to machining. Milling and grinding introduce an asymmetry into the symmetric rolling texture and residual stress state. After shot peening of cold-rolled specimens, a centrosymmetric residual stress state is found.

KEY WORDS: Surface texture, residual stresses, texture pole figures, lattice strain pole figures, machining, grinding, milling, shot peening.

INTRODUCTION

In many practical cases, the reliability and the functional behaviour of machined components is determined by the mechanical and structural properties of their surface layers (Macherauch *et al.*, 1987). This has, among others, been demonstrated for fatigue loaded parts as well as for parts sensitive to stress corrosion. Chip

forming as well as chipless machining procedures of metallic materials are always connected with elastic and plastic deformations, with the generation of heat and with the production of lattice imperfections in the near surface region. In general, the machining method applied and the machining parameters used determine together with the type and state of the material the properties of the very surface and of the subsurface areas. Besides of macroscopic changes of the dimensions of the workpiece, machining produces a characteristic surface topography, texture state and dislocation and twin density, changes in the coherency length and a typical micro- and macro-residual stress state. There exists a vast amount of informations about machining induced changes of topography, microstructure, hardness and residual stress distributions in the surface layers, especially with respect to the consequences of these items on the materials behaviour under fatigue loading. By way of contrast, however, only little knowledge exists about the development of machining textures and their consequences on the mechanical behaviour of materials (Wassermann and Grewen, 1962).

For instance, the changes of the near surface texture states in C 60 due to face milling and flat grinding were investigated (Fritsche *et al.*, 1979). In both cases asymmetric textures that could to a certain degree be correlated to cold rolling textures in the case of milling and hot rolling textures in the case of grinding were observed. The analogies were explained by the different amount of thermal energy dissipated into the surface layers of the material during both machining processes. Grinding textures in differently heat treated plain carbon steels were also investigated (Savchuck *et al.*, 1979). While the hardened material state showed no significant changes of the surface texture, weak symmetric machining textures were observed in the other cases. The individual texture components were described by ideal orientations as found in cold rolled and in recrystallized bcc-metals. The texture was considered as the result of normal and tangential forces as well as of partial recrystallization due to the grinding process.

Severely ground St 42 was found to exhibit a strong surface texture (Christian, 1971). In other experiments initial asymmetric grinding textures of Ck 45 showed characteristic changes as a consequence of wear (Krause and Mathias, 1983, Krause and Öcalan, 1984). Also in this case normal and tangential frictional

forces were discussed as decisive parameters for the texture alterations observed. Furthermore, asymmetric grinding textures were measured in differently manufactured silver polycrystals, in pure copper, in α-iron and in an austenitic steel (Hauk *et al.*, 1985). On the other hand, there also exist several investigations where no machining induced textures or changes of the initial texture state have been mentioned (Hauk *et al.*, 1985, Wolfstieg and Macherauch, 1976, Dölle and Cohen, 1980, Hauk *et al.*, 1980). For example, in a two phase CuAg-alloy no grinding texture was observed. In one case it was reported that a cold rolling texture disappeared in the near surface layers after grinding (Hauk and Stuitje, 1983).

Finally, for reasons of completeness it should be mentioned that shot peening develops centrosymmetric surface textures. In the case of Ck 45 and 16 MnCr 5 the heat treatment of the materials investigated was of considerable importance for the final texture state (Hoffmann, 1985).

Altogether it can be concluded that informations about textures formed by machining processes are scarce and far from being consistent. In most cases textures due to grinding have been investigated. However, sometimes the texture states existing before machining were not known. Thus, the correct assessment of machining induced changes in the orientation distribution of surface grains was not possible.

In this paper, the texture state and the lattice strain state of the near surface regions of specimens which were machined under specified conditions are analysed. Therefore, originally texture and residual stress free specimens as well as specimens with well defined texture and residual stress states before machining are investigated. In this way it will be demonstrated to which extent texture analyses and lattice strain determinations can provide useful informations for an improvement in realistically assessing machined surfaces of materials.

Material treatments and machining processes

The material investigated was a plain carbon steel (German grade Ck 45) with 0.5% C, 0.24% Si, 0.51% Mn, 0.005% P, 0.019% S, 0.1% Cr, balance Fe (all specifications in wt. – %). Two different

batches of specimens were machined. Specimens of the first batch had the dimensions $50 \times 30 \times 18\ mm^3$. In order to obtain a texture- and residual stress-free material state the specimens were quenched three times from 830°C in water of room temperature and finally normalized for 20 min at 830°. Specimens of the second batch had

Table 1 Process parameters used for the generation of machining textures

final machining condition	initial condition	machining parameters	
ground	normalized	up grinding	
		speed	28 m/s (40 1/s)
		cross-feed	8 mm
		1 cross-feed every two traverses	
		downfeed	6 μm
		total removal	0.5 mm
		wheel	Tyrolit 891746JV7217
milled	normalized	up milling	
		speed	12 m/min (63 1/min)
		feed	20 mm/min
		depth of cut	1.5 mm
		HSS peripheral mill ∅61.5 mm	
		axial rake angle 40°	
		8 teeth	
shot peened	normalized	air blast method	
		pressure	1.6 bar
		shot	S 170
		coverage	100%
cold rolled and milled	78% cold rolled	up milling	
		speed	12 m/min (38 1/min)
		feed	20 mm/min
		depth of cut	0.3 mm
		HSS peripheral mill ∅100 mm	
		axial rake angle ±14.5°	
		24 teeth	
cold rolled and ground	78% cold rolled	up grinding	
		speed	28 m/s (40 1/s)
		cross-feed	8 mm
		1 cross-feed every two traverses	
		downfeed	6μm
		total removal	0.5 mm
		wheel	Tyrolit 891746JV7217
cold rolled and shot peened	78% cold rolled	air blast method	
		pressure	1.6 bar
		shot	S 170
		coverage	100%

the dimensions $100 \times 30 \times 5\ mm^3$. After recrystallization at 650°C for 2 h in vacuum, followed by furnace cooling, the specimens were cold rolled on a laboratory rolling mill with 0.2 mm reduction/pass. The final thickness was 1.1 mm, corresponding to a rolling deformation of 78%. In this way a typical cold rolling texture and residual stress state was generated.

Normalized specimens and cold rolled specimens were milled, ground or shot peened. The parameters used in the machining processes are compiled in Table 1. Surface layers of the normalized specimens that might have suffered decarburization or oxidation during the hardening and normalizing treatment were removed by the subsequent machining process or by electropolishing.

X-RAY MEASUREMENTS

Figure 1 shows a specimen and the appertaining system of coordinates that in the following will be referred to. LD, RD and

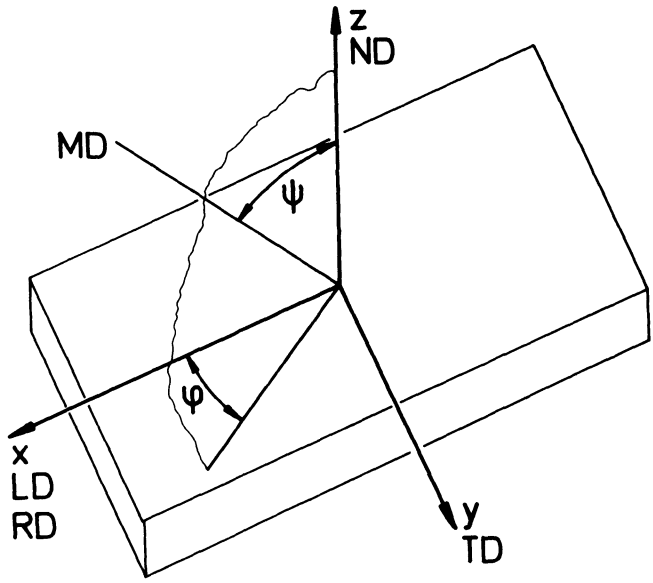

Figure 1 Specimen coordinate system used for the definition of the angles φ and ψ

TD are the longitudinal, rolling and transverse direction, respectively. ND indicates the direction of a normal to the specimen surface. The feed direction in milling and the traverse direction in grinding coincide with the longitudinal direction. The shot peening direction is the normal direction.

MD, defined by the variable angles φ and ψ is a measuring direction of lattice deformations and pole densities by X-ray diffraction. For that purpose, an X-ray source has to be positioned in such a way that the $\{hkl\}$-directions of diffracting lattice planes $\{hkl\}$ coincide with MD. Lattice strain and texture states were determined with a stress-texture ψ-diffractometer, equipped with a position sensitive detector (Hoffmann *et al.*, 1985).

The measurements performed covered the intervals of $-70° \leqslant \psi \leqslant 70°$ and $0° \leqslant \varphi \leqslant 350°$ in steps of $\Delta\varphi = \Delta\psi = 10°$. Always {110}- and {211}-lattice planes were measured with CrKα-radiation. A vanadium filter was used for the elimination of the CrKβ-radiation.

The surface texture state of the machined specimens was evaluated from the integrated intensities of {110} and {211} interference lines measured in the φ, ψ-intervals mentioned above. The integrated intensity is determined as the area delimited by the interference profile above a threshold level of 20% of the maximum peak height after background subtraction. Textures will be characterized in the classical way by pole figures. Due to the limitation of the range of measuring directions to a maximum value of $|\psi| = 70°$, the pole figures shown in this paper are also limited by the stereographic projection of a small circle that corresponds to a tilt angle of $|\psi| = 70°$. In order to characterize the strength of a texture state, the ratio I_{max}/I_{min} of the largest to the smallest number of counts (cts) appearing within the measuring range shown in the pole figures is calculated. This may lead to difficulties if I_{min} is very small. However, the use of the intensity ratio is reasonable in the present case, because the textures observed in the experiments presented in this paper were not very strong and sufficient X-ray intensity was always found also in regions of minimum pole density. If $I_{max}^{\{110\}}/I_{min}^{\{110\}} < 10$, a texture is called weak in this paper.

Using a system of coordinates oriented as shown in Figure 1 the linear theory of elasticity yields the following relation between the

lattice strains $\varepsilon_{\varphi,\psi}$ in the directions φ, ψ, the stress components σ_{xx}, σ_{yy}, σ_{zz}, τ_{xy}, τ_{xz}, τ_{yz} and the elastic constants s_1 and $\frac{1}{2}s_2$:

$$\varepsilon_{\varphi,\psi} = \tfrac{1}{2}s_2(\sigma_{xx}\cos^2\varphi + \sigma_{yy}\sin^2\varphi + \tau_{xy}\sin 2\varphi)\sin^2\psi + \tfrac{1}{2}s_2\sigma_{zz}\cos^2\psi + \tfrac{1}{2}s_2(\tau_{xz}\cos\varphi + \tau_{yz}\sin\varphi)\sin 2\psi + s_1(\sigma_{xx} + \sigma_{yy} + \sigma_{zz}) \quad (1)$$

s_1 and $\frac{1}{2}s_2$ are functions of the Miller indices of the measured $\{hkl\}$-planes and the elastic properties of the grains of the polycrystals investigated. Such X-ray elastic constants can be calculated from single crystal compliances s_{ik} by the aid of the hypotheses of (Voigt, 1928) and (Reuß, 1929). With appropriate s_{ik}-values (Bechmann and Hearmon, 1966) the average of the values $\frac{1}{2}s_2$ and s_1 obtained with (Voigt, 1928) and (Reuss, 1929) follow as

$$s_1 = -1.274 \cdot 10^{-6}\,\text{mm}^2/\text{N}$$
$$\tfrac{1}{2}s_2 = 5.767 \cdot 10^{-6}\,\text{mm}^2/\text{N} \quad (2)$$

for measurements of {211}-lattice planes. According to Bragg's law the lattice strain $\varepsilon_{\varphi,\psi}$ can be correlated with lattice spacings $D_{\varphi,\psi}$ and Bragg-angles $2\theta_{\varphi,\psi}$ respectively by

$$\varepsilon_{\varphi,\psi} = \frac{D_{\varphi,\psi} - D_0}{D_0} = -\tfrac{1}{2}\cot\theta_0 \cdot (2\theta_{\varphi,\psi} - 2\theta_0) \quad (3)$$

D_0 and $2\theta_0$ are the respective values of the stress free material state.

The correct magnitudes of the stress components σ_{xx}, σ_{yy} and σ_{zz} in the diffracting volume can only be determined if the appertaining value of D_0 or $2\theta_0$ respectively is known. Under the assumption that the principal stresses σ_I and σ_{II} are parallel to the specimen surface the stress components τ_{xz} and τ_{yz} are zero with respect to the coordinate system shown in Figure 1. Eq. (1) reduces then to

$$\varepsilon_{\varphi,\psi} = \tfrac{1}{2}s_2(\sigma_\varphi - \sigma_{zz})\sin^2\psi + s_1(\sigma_{xx} + \sigma_{yy}) + (s_1 + \tfrac{1}{2}s_2)\sigma_{zz} \quad (4)$$

with

$$\sigma_\varphi = \sigma_{xx}\cos^2\varphi + \sigma_{yy}\sin^2\varphi + \tau_{xy}\sin 2\varphi \quad (5)$$

σ_φ is the normal stress acting in the azimuth φ. As can be seen,

only the stress $(\sigma_\varphi - \sigma_{zz})$ can be obtained from the slope of a straight line fit to the $\varepsilon_{\varphi,\psi}$-$\sin^2\psi$-distribution measured in the azimuth φ. Here the knowledge of D_0 or $2\theta_0$ is of minor importance because only the slope but not the absolute position of the $\varepsilon_{\varphi,\psi}$-$\sin^2\psi$ distribution is used. But the stress component σ_{zz} is related to the intercept of the $\varepsilon_{\varphi,\psi}$-$\sin^2\psi$-distribution with the ordinate axis at $\psi = 0°$, and can only be determined if D_0 or $2\theta_0$ is known. Mostly, this is not the case. The experimental determination of D_0 and $2\theta_0$ requires considerable experimental effort. Furthermore, the application of values of D_0 or $2\theta_0$ that have been deduced from measurements on stress-free specimens to the evaluation of residual stresses in other specimens of the same material is not free of uncertainties. The processes that caused the residual stress state to be investigated may have also changed the material state in such a manner as to exhibit a different D_0 or $2\theta_0$ compared to the residual stress free material state. Thus large errors may occur in the determined stress components σ_{zz} due to errors in D_0 or $2\theta_0$ respectively.

In many cases, however, it can reasonably be assumed that σ_{zz} is negligible. Then Eq. (4) reduces further to the basic relation of the classical $\sin^2\psi$ method (Macherauch and Müller, 1961)

$$\varepsilon_{\varphi,\psi} = \tfrac{1}{2}s_2\sigma_\varphi \sin^2\psi + s_1(\sigma_{xx} + \sigma_{yy}) \tag{6}$$

If the principal stresses σ_I and σ_{II} are not surface parallel then the shear stress components τ_{xz} and τ_{yz} attain non-zero values with respect to the specimen coordinate system. The determination of the six independent stress components σ_{xx}, σ_{yy}, σ_{zz}, τ_{xy}, τ_{xz} and τ_{yz} can then e.g. follow procedures proposed by (Dölle and Hauk, 1976) or (Wagner *et al.*, 1983). Following (Wagner *et al.*, 1983), Eq. (1) can be transformed using Hooke's law, into

$$\begin{aligned}\varepsilon_{\varphi,\psi} = {} & (\varepsilon_{xx}\cos^2\varphi + \varepsilon_{yy}\sin^2\varphi + \varepsilon_{xy}\sin 2\varphi)\sin^2\psi + \\ & + \varepsilon_{zz}\cos^2\psi + (\varepsilon_{xz}\cos\varphi + \varepsilon_{yz}\sin\varphi)\sin 2\psi\end{aligned} \tag{7}$$

By writing Eq. (7) in the form

$$\varepsilon_{\varphi,\psi} = \tfrac{1}{2}A_0^\psi + A_1^\psi\cos\varphi + A_2^\psi\cos 2\varphi + B_1^\psi\sin\varphi + B_2^\psi\sin 2\varphi \tag{8}$$

it can be looked upon as a Fourier series. The strain components ε_{xx}, ε_{yy}, ε_{zz}, ε_{xy}, ε_{xz} and ε_{yz} are related to the Fourier coefficients

A_0^ψ, A_1^ψ, A_2^ψ, B_1^ψ and B_2^ψ which can be calculated using the measured values of $\varepsilon_{\varphi,\psi}$. With Hooke's law the stress components σ_{xx}, σ_{yy}, σ_{zz}, τ_{xy}, τ_{xz} and τ_{yz} can be calculated.

In this paper values of $\varepsilon_{\varphi,\psi}$ measured in 253 different directions φ, ψ were used for the determination of the near surface residual stress states. Stress values $\leqslant 10\,\mathrm{N/mm^2}$ are within the limits of experimental accuracy and are considered as negligible.

The assumption of isotropic or quasiisotropic material behaviour is no more fulfilled in the presence of texture states. Then the X-ray elastic constants depend on the measuring directions φ, ψ and the conventional methods of X-ray stress analysis are no longer applicable. A pragmatical overcoming of this problem is in the case of steels achieved by measuring {732/651}-lattice planes with MoKα-radiation where linear lattice strain distributions have frequently been found also in texturized material states (Maurer *et al.*, 1987, Hauk *et al.*, 1985). However, as shown for cold rolled material states like those discussed in this paper (Maurer *et al.*, 1987) as well as for others (Hauk *et al.*, 1985) the evaluation of nonlinear lattice strain distributions measured at {211}-lattice planes by the aid of the conventional method with quasiisotropic X-ray elastic constants yields residual stress values which agree quite well with those obtained from linear lattice strain distributions observed at {732/651}-lattice planes. This is in particular valid for weak textures observed in the machined surfaces investigated in this paper if the measurement of lattice strains is extended to large angles $|\psi| > 45°$.

Consequently, surface residual stress components will in this paper be determined according to (Macherauch and Müller, 1961) and (Wagner *et al.*, 1983) with quasiisotropic X-ray elastic constants (Eq. 2) from the lattice strains $\varepsilon_{\varphi,\psi}$ measured at {211}-lattice planes.

The surface residual lattice strain states will be represented graphically by the aid of lattice deformation pole figures (Hoffmann *et al.*, 1983). For that purpose the lattice spacing $D_{\varphi,\psi}^{\{211\}}$ measured in the directions φ, ψ is converted to the spacing of {100}-lattice planes by

$$D_{\varphi,\psi}^{\{100\}} = \frac{D_{\varphi,\psi}^{\{211\}}}{\sqrt{6}} = a_{\varphi,\psi} \tag{9}$$

Instead of the lattice strain $(a_{\varphi,\psi} - a_0)/a_0$ the lattice deformation state is characterized by the lattice spacings $a_{\varphi,\psi}$. They are plotted in stereographic projection and points with equal values of $a_{\varphi,\psi}$ are connected by contour lines. Like texture pole figures the lattice deformation pole figures are limited to $|\psi| \leq 70°$. Nonetheless, the directions LD, TD indicated at the outer boundary of all pole figures include an angle of 90° and are also perpendicular to ND, the stereographically projected pole of which is the center of each pole figure.

EXPERIMENTAL RESULTS AND DISCUSSION

Normalized and cold rolled material states

X-ray measurements at {110}- and {211}-lattice planes proved that the normalized specimens were free of residual stresses and texture. The integral intensities of the appertaining interference lines were nearly constant. With the experimental set up used a mean intensity of $I^{\{110\}} = 1566 \pm 75$ counts/s was observed at {110}-lattice planes.

From the measured $D_{\varphi,\psi}^{\{211\}}$-values in all directions φ, ψ a mean $D_0^{\{100\}}$-value

$$D_0^{\{100\}} = a_0 = 0.28666 \pm 0.00008 \text{ nm} \tag{10}$$

was obtained. Only statistical and no systematic deviations from the mean value occurred. $D_0^{\{100\}}$ is equal to the lattice constant a_0.

The {110}- and {211}-surface texture pole figures of a 78% cold rolled specimen are shown in Figures 2a and 2b. The ratio I_{max}/I_{min} between the maximum and minimum intensities is for {110}-planes 7.47 and for {211}-planes 1.93. The texture state can be characterized by a typical cold rolling texture (Wassermann and Grewen, 1962).

The near surface residual strain state of 78% cold rolled specimens measured at {211}-lattice planes is represented by the lattice deformation pole figure (a-distributions) shown in Figure 3a. $a_{\varphi,\psi}$ vs. $\sin^2\psi$ distributions in the azimuth $\varphi = 0°$ and 90° are illustrated in Figure 3b for positive and negative ψ-values. It is important to note that the distributions do not reveal any ψ-splitting but considerable non-linearities, especially in the azimuth

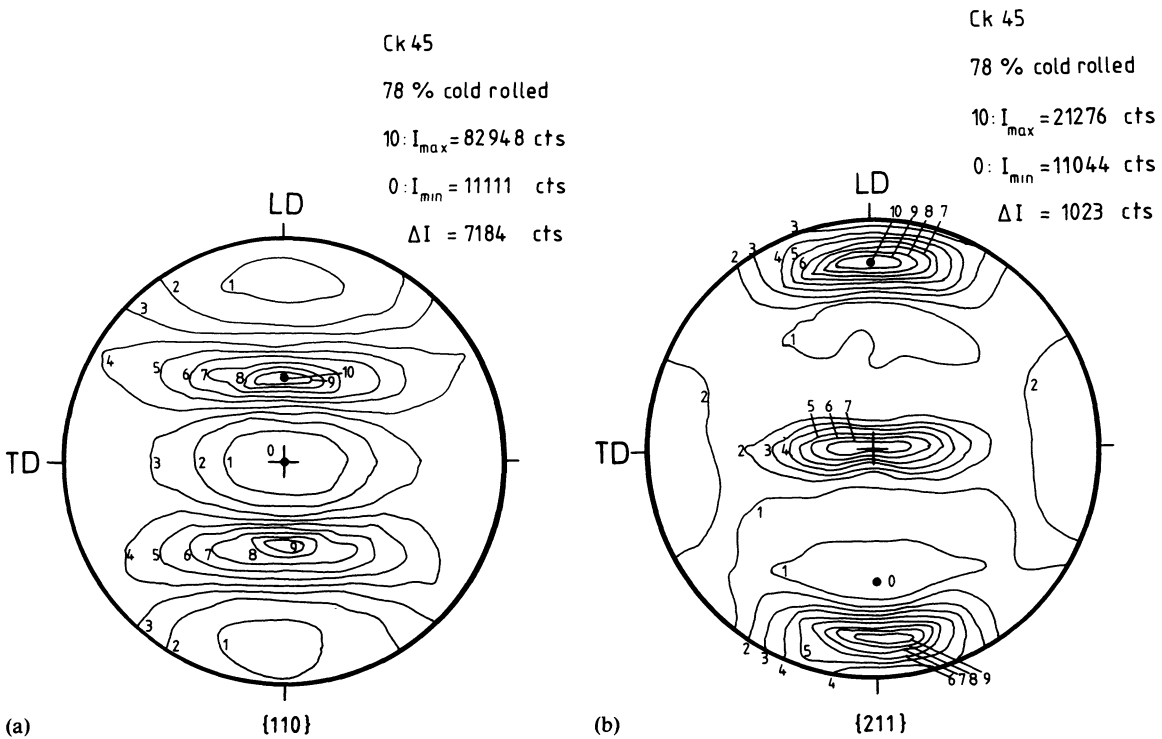

Figure 2 (a) {110}- and (b) {211}-texture pole figures after 78% cold rolling ($0° \leq \psi \leq 70°$)

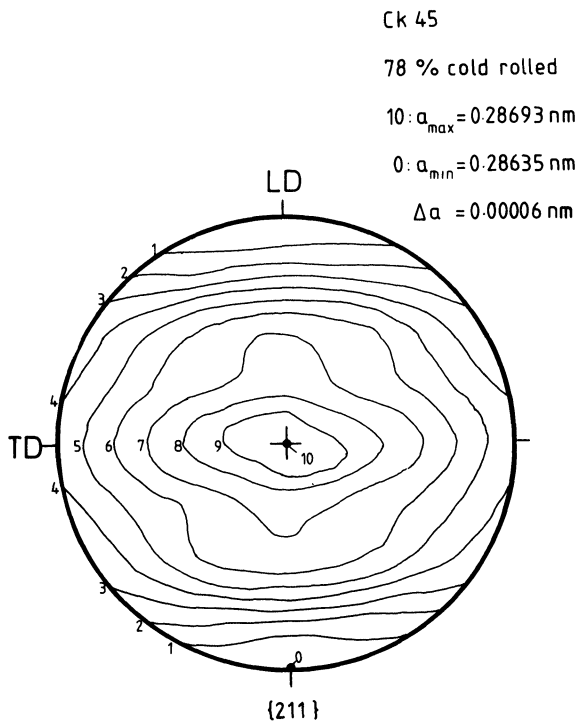

Figure 3 (a) Lattice deformation pole figure of {211}-lattice planes after 78% cold rolling (surface) ($0° \leq \psi \leq 70°$)

$\varphi = 0°$. If a biaxial surface residual stress state with principal stresses of equal sign but different quantities would exist, linearily distributed a-values in all azimuths φ and a lattice deformation pole figure with elliptical contour lines would be expected. The deviations observed from this behaviour which can clearly be seen in Figure 3a and Figure 3b are due to texture effects.

By evaluating the lattice deformation distribution given in Figure 3a the stress tensor

$$\sum = \begin{pmatrix} -324 & 0 & 0 \\ 0 & -170 & 0 \\ 0 & 0 & 66 \end{pmatrix} \text{N/mm}^2 \qquad (11)$$

is obtained if the X-ray elastic constants and the value of a_0

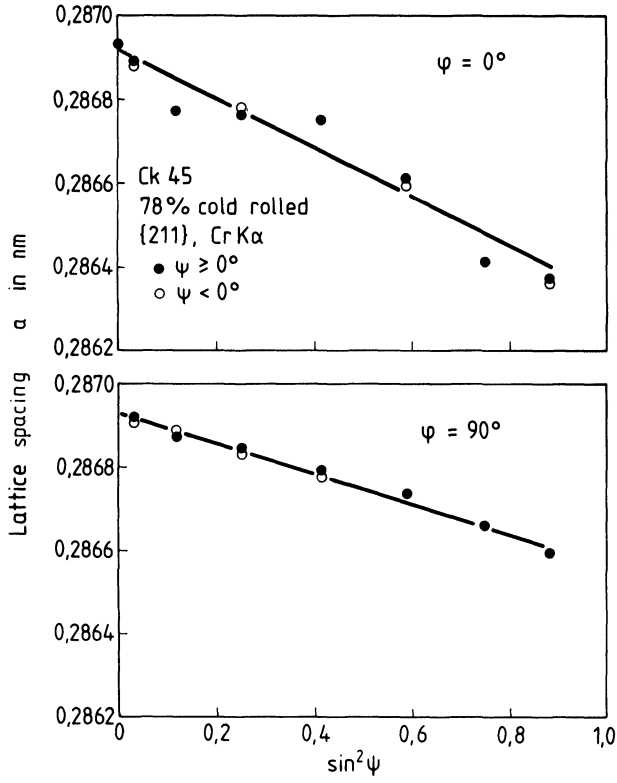

Figure 3 (b) a vs. $\sin^2 \psi$ distributions in the azimuths $\varphi = 0°$ and $\varphi = 90°$ of the pole figure shown in (a) (surface)

mentioned above are used. The system of the principal stresses $\sigma_I = 66\,\mathrm{N/mm^2}$, $\sigma_{II} = -170\,\mathrm{N/mm^2}$ and $\sigma_{III} = -324\,\mathrm{N/mm^2}$ coincides with the specimen system.

Since the surface layer is removed by grinding and milling the texture found after grinding has to be compared to the texture state that is representative for the depth to which the material is removed. Figure 4 shows the {110}- and {211}-texture pole figures of a cold rolled specimen after electrolytically removing a layer of 0.12 mm thickness. The pole density distribution and the intensity ratios are slightly different to that found at the surface. For the {110}-pole figures the intensity ratio $I_{max}/I_{min} = 9.96$ and for the

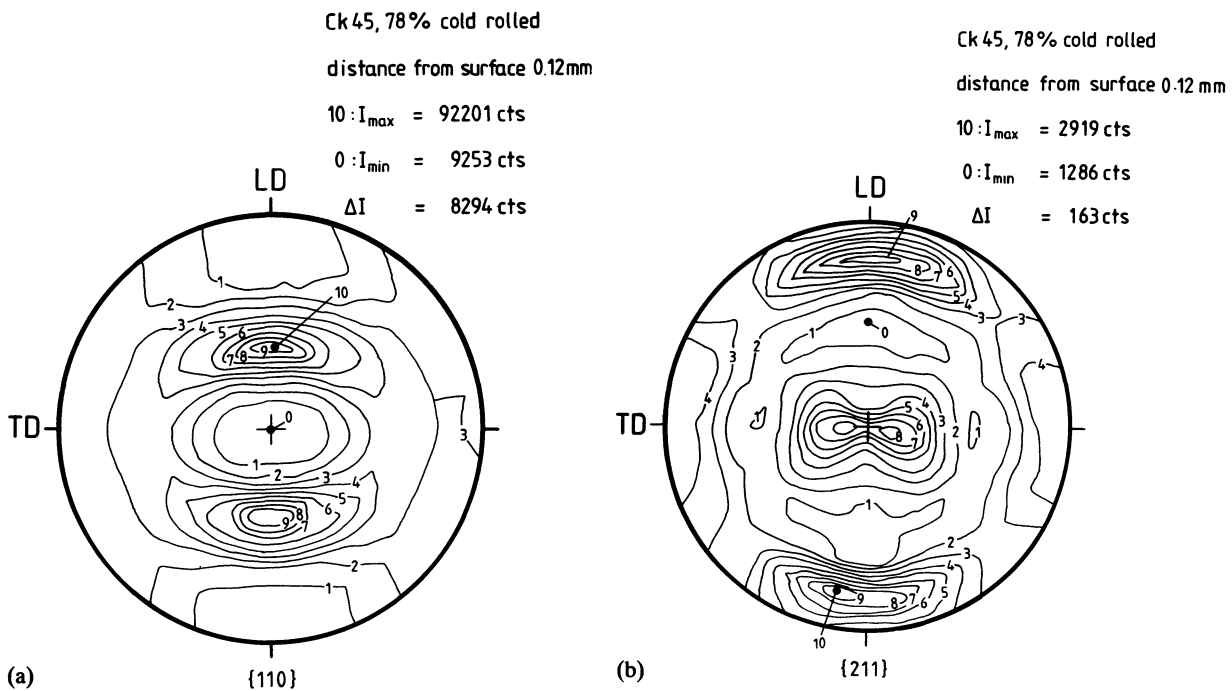

Figure 4 (a) {110}- and (b) {211}-texture pole figures of a cold rolled specimen in a surface distance of 0.12 mm ($0° \leq \psi \leq 70°$)

{211}-pole figures $I_{max}/I_{min} = 2.27$ is observed. Obviously, the texture in the interior of the specimen is stronger than at the very surface. Figure 5 displays the lattice deformation state measured at {211}-lattice planes in a depth of 0.12 mm. Comparing the a-pole figure (Figure 5a) and the appertaining a vs. $\sin^2\psi$ distributions in the azimuths $\varphi = 0°$ and $\varphi = 90°$ (Figure 5b) to those shown in Figure 3, a similarity can be stated. However, evaluating the lattice deformation state of Figure 5a, the stresses

$$\sum = \begin{pmatrix} -293 & 0 & 0 \\ 0 & -134 & 0 \\ 0 & 0 & 0 \end{pmatrix} \text{N/mm}^2 \tag{12}$$

are obtained. They are considerably smaller than in the very

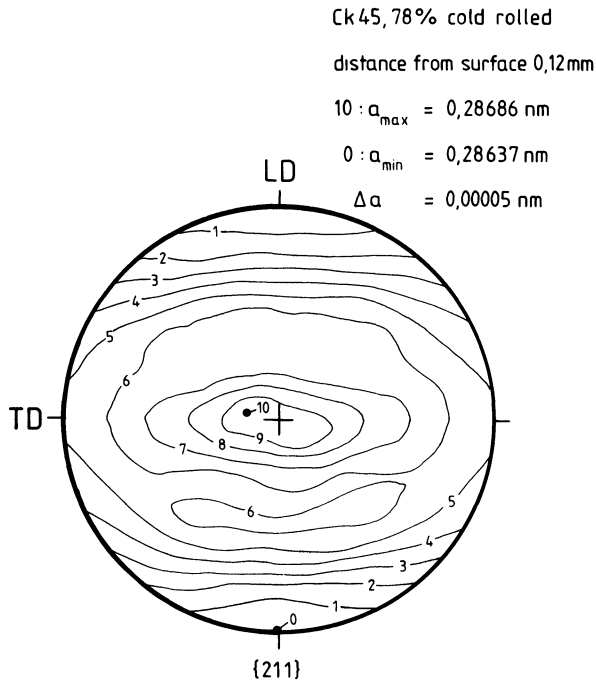

Figure 5 (a) Lattice deformation pole figure measured at {211}-lattice planes of a 78% cold rolled specimen in a surface distance of 0.12 mm ($0° \leq \psi \leq 70°$)

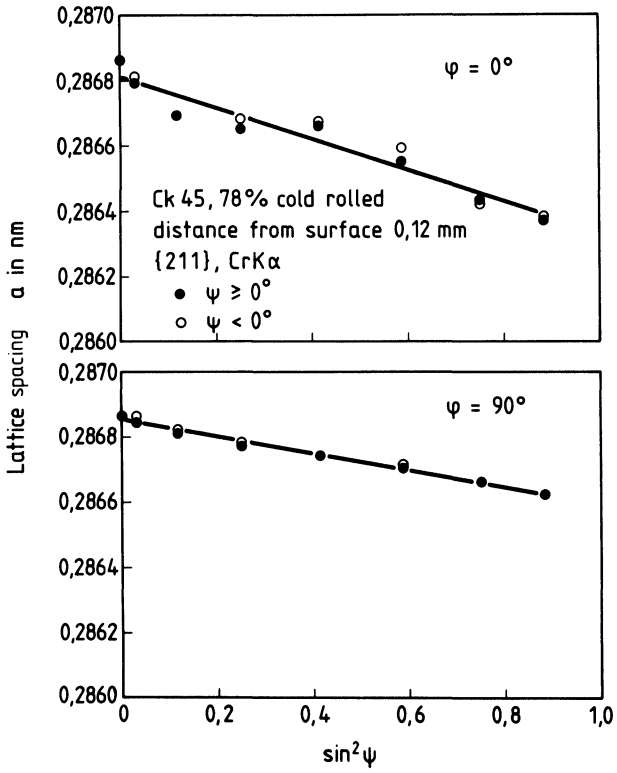

Figure 5 (b) a vs. $\sin^2 \psi$ distributions in the azimuths $\varphi = 0°$ and $\varphi = 90°$ of the pole figure shown in (a)

surface. Furthermore, no σ_{zz}-component is prevalent in the diffracting volume.

MILLING OF NORMALIZED AND COLD ROLLED MATERIAL STATES

The near surface texture state of a normalized specimen after milling characterized by the {110}- and {211}-texture pole figures is presented in Figure 6. The milling process produced a characteristic texture, whose prominent feature is its asymmetry with regard to

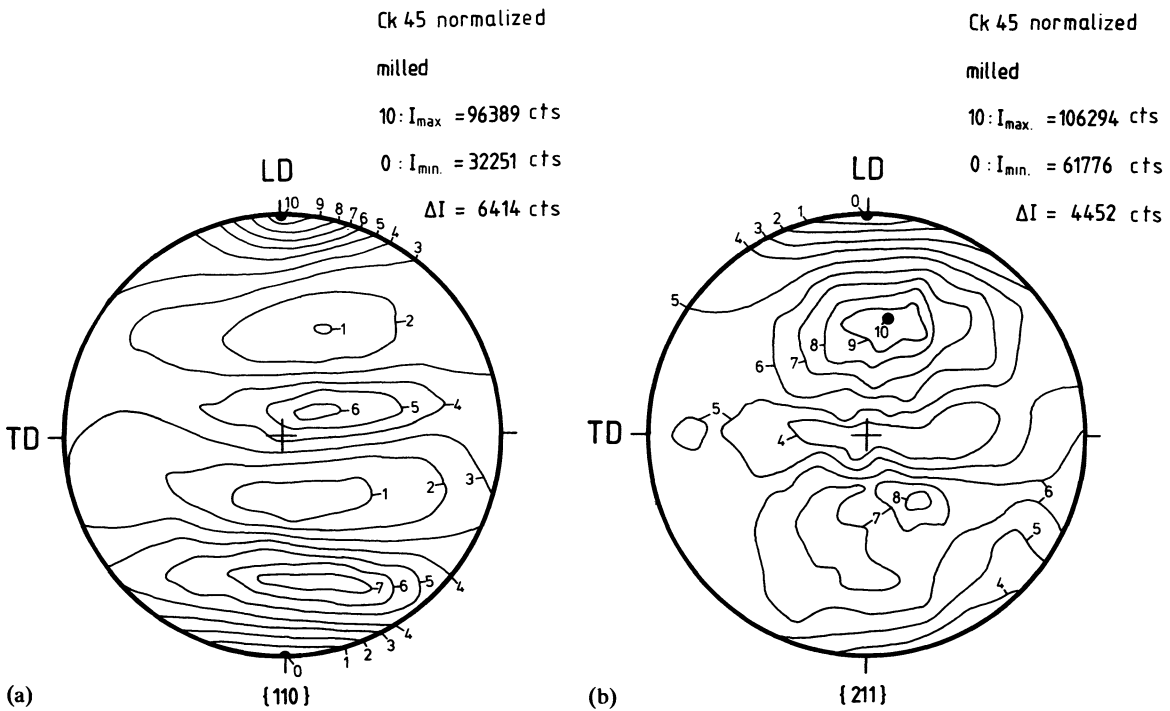

Figure 6 (a) {110}- and (b) {211}-texture pole figures after milling of a normalized specimen ($0° \leq \psi \leq 70°$)

the longitudinal as well as to the transverse direction. This asymmetry is caused by the cutting forces exerted by the milling tool. Due to the axial rake angle of the cutter (see Table 1) the resulting cutting forces acting in the specimen surface are inclined at a certain angle to the feed direction which is identical with the specimens longitudinal direction. The ratio $I_{max}/I_{min} = 2.99$ in the {110}-pole figure and $I_{max}/I_{min} = 1.72$ in the {211}-pole figure indicates that the milling texture observed is only weak.

The near surface lattice strain state of a normalized specimen after milling is shown in Figure 7. While Figure 7a displays the pole figure of the a values derived from measurements at {211}-lattice planes, Fig. 7b represents a-sin$^2\,\psi$ distributions in sections $\varphi = 0°$ and $\varphi = 90°$ of Figure 7a.

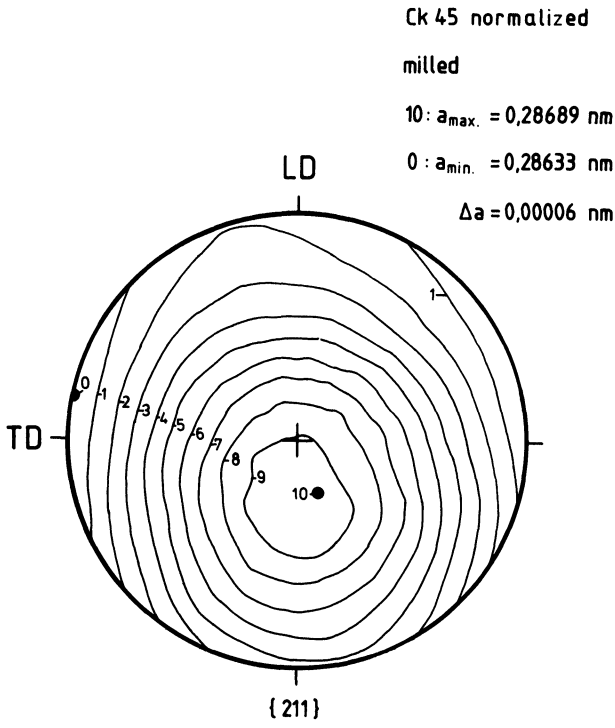

Figure 7 (a) Lattice deformation pole figure measured at {211} lattice planes after milling of a normalized specimen ($0° \leq \psi \leq 70°$)

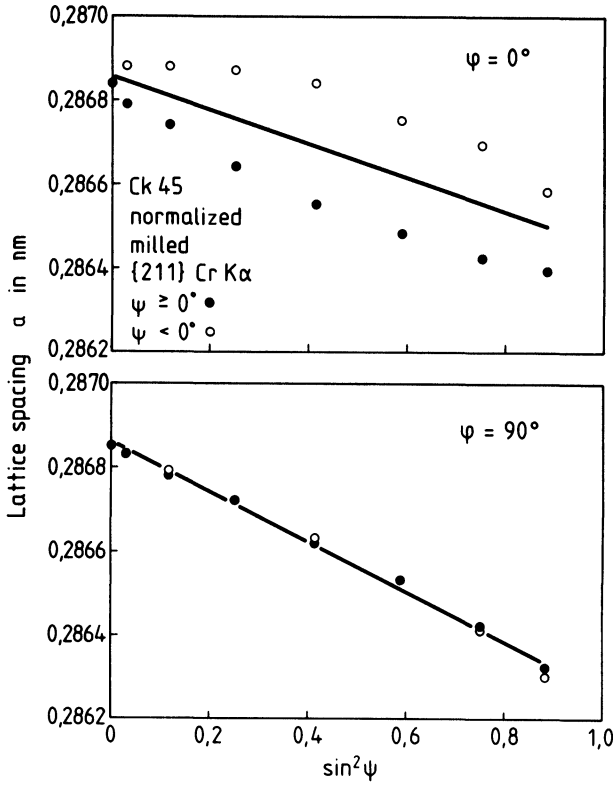

Figure 7 (b) a vs. $\sin^2 \psi$ distributions in the azimuths $\varphi = 0°$ and $\varphi = 90°$ of the pole figure shown in (a)

Just as the texture pole figures (Figure 6) the pole figure of the a-values reveals an asymmetry with regard to the longitudinal and the transverse direction. The contour line spacing in the azimuth $\varphi = 90°$ is almost equidistant in the angular range $20° \angle \psi \angle 60°$ indicating an approximately linear a vs. $\sin^2 \psi$ distribution. In the azimuth $\varphi = 0°$ ψ-splitting of the a values is observed. Despite of the preferred orientation of the grains, no correlation can be detected between the texture state and the lattice deformation state (see Figure 6b). The residual stress state can be determined according to Eq. (8) using the X-ray elastic constants given by Eq.

(2). With the lattice constant a_0 determined in the normalized stress- and texture-free material state, the tensor

$$\sum = \begin{pmatrix} -252 & 14 & -77 \\ 14 & -360 & 0 \\ -77 & 0 & -24 \end{pmatrix} \text{N/mm}^2 \tag{13}$$

is obtained. As can be seen the applied milling procedure generates in specimens compressive normal stresses σ_{xx} and σ_{yy} whose magnitudes are larger in the transverse than in the longitudinal direction. The shear stress components τ_{xy} and τ_{xz} are responsible for the observed asymmetry of the distribution of the a-values in the lattice deformation pole figure with respect to the transverse and longitudinal direction, however, τ_{zx} to a larger extent that τ_{xy}. Also within the penetration depth of the X-rays a small but not negligible value of σ_{zz} is observed.

The stress state given by this tensor (Eq. 13) has principal axes that are inclined to the specimen coordinate system. To a good approximation the principal system is obtained by first rotating the specimen coordinate system counterclockwise by 10° about the normal direction. A second rotation of −17° about the new position of the transverse direction of the rotated specimen coordinate system leads to the principal system. The principal stress tensor is

$$\sum^P = \begin{pmatrix} -273 & 0 & 0 \\ 0 & -362 & 0 \\ 0 & 0 & 0 \end{pmatrix} \text{N/mm}^2 \tag{14}$$

The texture state and the lattice deformation state after milling of a cold rolled specimen is shown in Figure 8 and Figure 9. After milling the intensity ratio is $I_{max}/I_{min} = 2.71$ for the {110}-pole figure and $I_{max}/I_{min} = 1.63$ for the {211}-pole figure. Compared to the texture state after cold rolling (Figure 4) the intensity ratio has been diminished in both pole figures by milling. Also the shape of the pole density distribution has changed. This is more pronounced in the {110}-pole figure (Figure 8a) where a marked asymmetry with respect to TD can be seen. This asymmetry is also found in the lattice deformation pole figure shown in Figure 9. Despite of the strong texture related anomalies that are present in the cold rolled state (Figure 5), these are considerably weaker after milling. The *a*

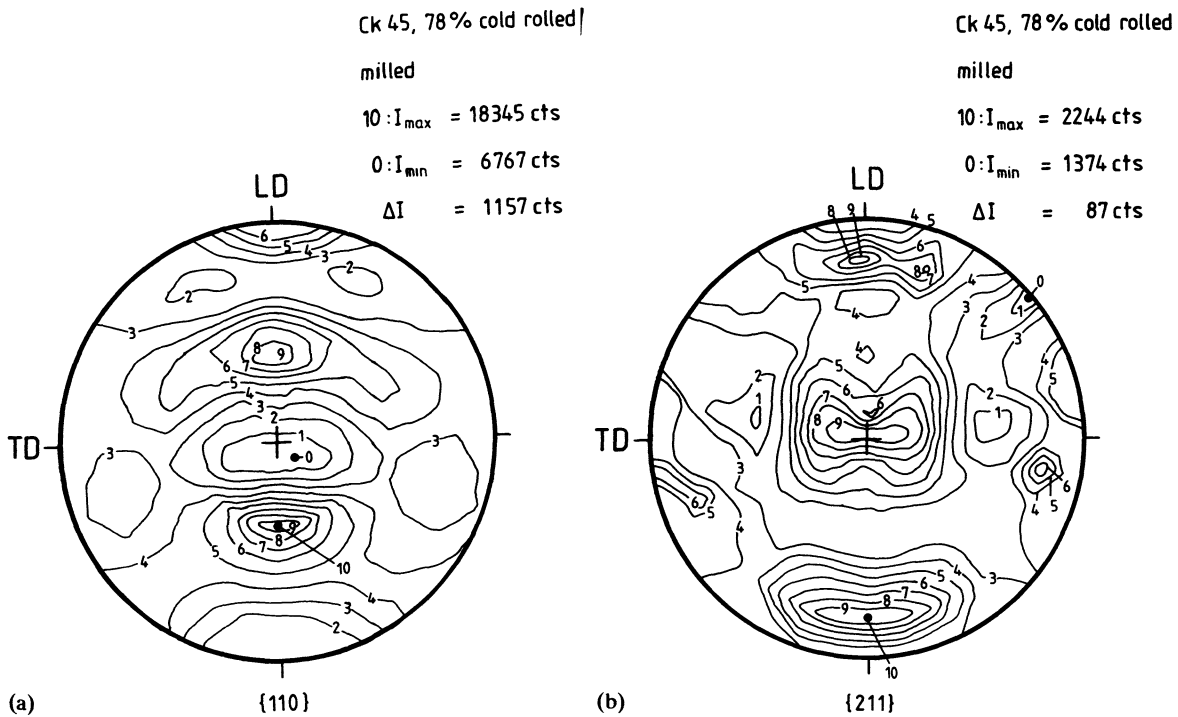

Figure 8 (a) {110}- and (b) {211}- texture pole figures after milling of a cold rolled specimen ($0° \leq \psi \leq 70°$)

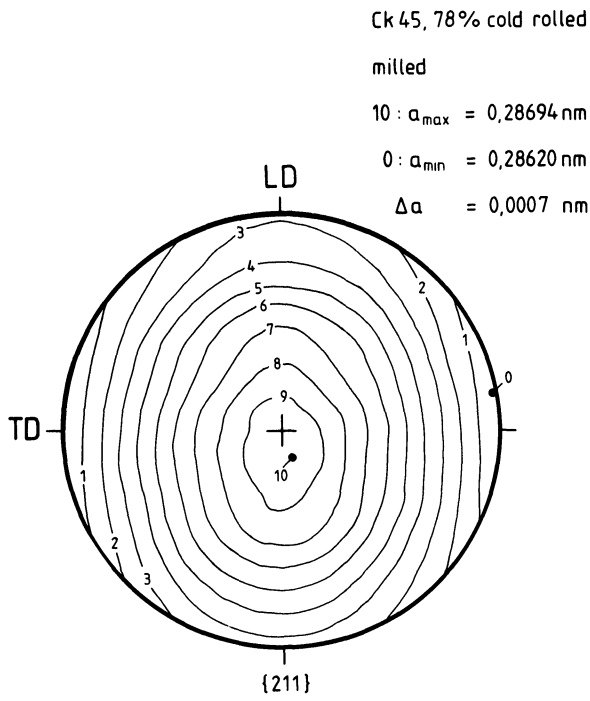

Figure 9 (a) Lattice deformation pole figure measured at {211}-lattice planes after milling of a cold rolled specimen ($0° \leq \psi \leq 70°$)

vs. $\sin^2 \psi$ distribution given in Figure 9b reveals that ψ-splitting exists in the azimuth $\varphi = 0°$ but not in the azimuth $\varphi = 90°$. It also shows that the texture-related anomalies are still preserved after milling and have qualitatively the same shape as after cold rolling (Figure 5b).

Evaluating the lattice deformation distribution given in Fig. 9a with the X-ray elastic constants and the value of a_0 given above the stress tensor

$$\Sigma = \begin{pmatrix} -357 & -3 & -37 \\ -3 & -521 & 0 \\ 37 & 0 & -46 \end{pmatrix} \simeq \begin{pmatrix} -357 & 0 & -37 \\ 0 & -521 & 0 \\ -37 & 0 & -46 \end{pmatrix} \text{N/mm}^2 \quad (15)$$

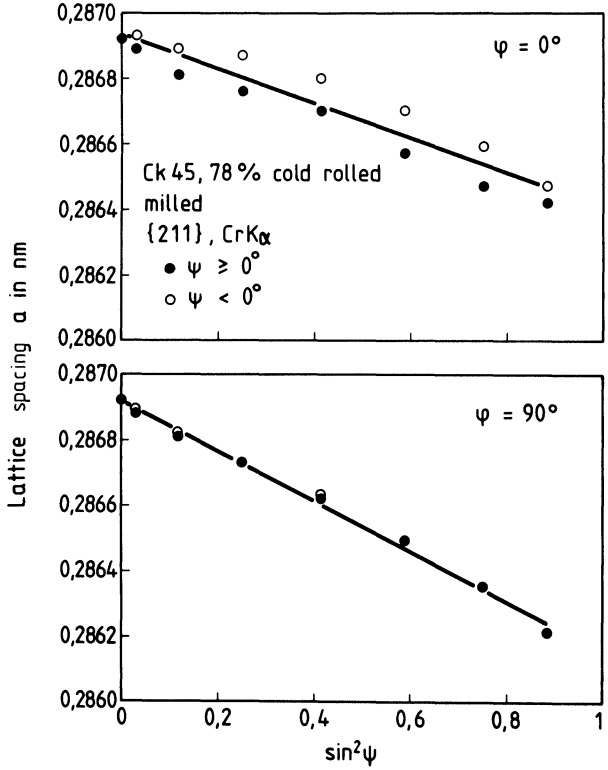

Figure 9 (b) a vs. $\sin^2 \psi$ distributions in the azimuths $\varphi = 0°$ and $\varphi = 90°$ of the pole figure shown in (a)

is obtained. The only non-vanishing shear stress component is τ_{xz}. There also exists, like in the normalized and milled specimen, a surface normal stress σ_{zz} within the diffracting volume. The normal stress σ_{xx} has a smaller magnitude than the normal stress σ_{yy}. The principal system is rotated by $-7°$ about TD with respect to the specimen system. With respect to the principal system, the stress tensor given above transforms into the tensor of the principal stresses

$$\Sigma^P = \begin{pmatrix} -361 & 0 & 0 \\ 0 & -521 & 0 \\ 0 & 0 & -42 \end{pmatrix} \text{N/mm}^2 \qquad (16)$$

The difference between the symmetry of the pole density distributions with respect to the specimen system observed after milling of a normalized (Figure 7) and of a cold rolled specimen (Figure 9) can be explained by the differences in the milling tool. While in milling of the normalized specimen, the cutting teeth of the milling tool had an axial rake angle of +40°, the peripheral mill used in milling the cold rolled specimen had teeth with axial rake angles which were intermittendly +14.5° or −14.5°. Thus, tangential cutting forces acting perpendicular to LD change their direction at every other tooth. It is to be expected that these cutting forces average to zero and cannot cause texture states and residual stress states that are asymmetric with respect to LD as in the milled normalized specimen.

GRINDING OF NORMALIZED AND COLD ROLLED MATERIAL STATES

In Figure 10 the {110}- and {211} texture pole figures of normalized Ck 45 specimens after grinding are shown. The orientation distributions measured at both types of lattice planes are almost symmetric with respect to LD but asymmetric with respect to TD. The intensity ratio in the {110}-pole figure is $I_{max}/I_{min} = 1.93$, in the {211}-pole figure $I_{max}/I_{min} = 1.43$, again indicating a weak texture.

The asymmetry with respect to TD is also found in the a-pole figure presented in Figure 11a. As can be seen from Figure 11b ψ-splitting is observed in the section $\varphi = 0°$ of the a-pole figure but not in the section $\varphi = 90°$.

The larger curvature of the measured a-values vs. $\sin^2\psi$ for positive and negative ψ-values at $\varphi = 90°$ in comparison to that of the milled specimen in Figure 7b has to be attributed to a stronger stress gradient $d\sigma_{yy}/dz$ (Hauk and Vaessen, 1983). Approximating the measured a vs. $\sin^2\psi$ values by the straight lines drawn in Fig. 11b the stress tensor components according to (Wagner *et al.*, 1983) using the X-ray elastic constants and the value of a_0 mentioned above, are

$$\Sigma = \begin{pmatrix} -253 & -6 & -58 \\ -6 & -438 & 0 \\ -58 & 0 & -105 \end{pmatrix} \simeq \begin{pmatrix} -253 & 0 & -58 \\ 0 & -438 & 0 \\ -58 & 0 & -105 \end{pmatrix} (\mathrm{N/mm^2}) \tag{17}$$

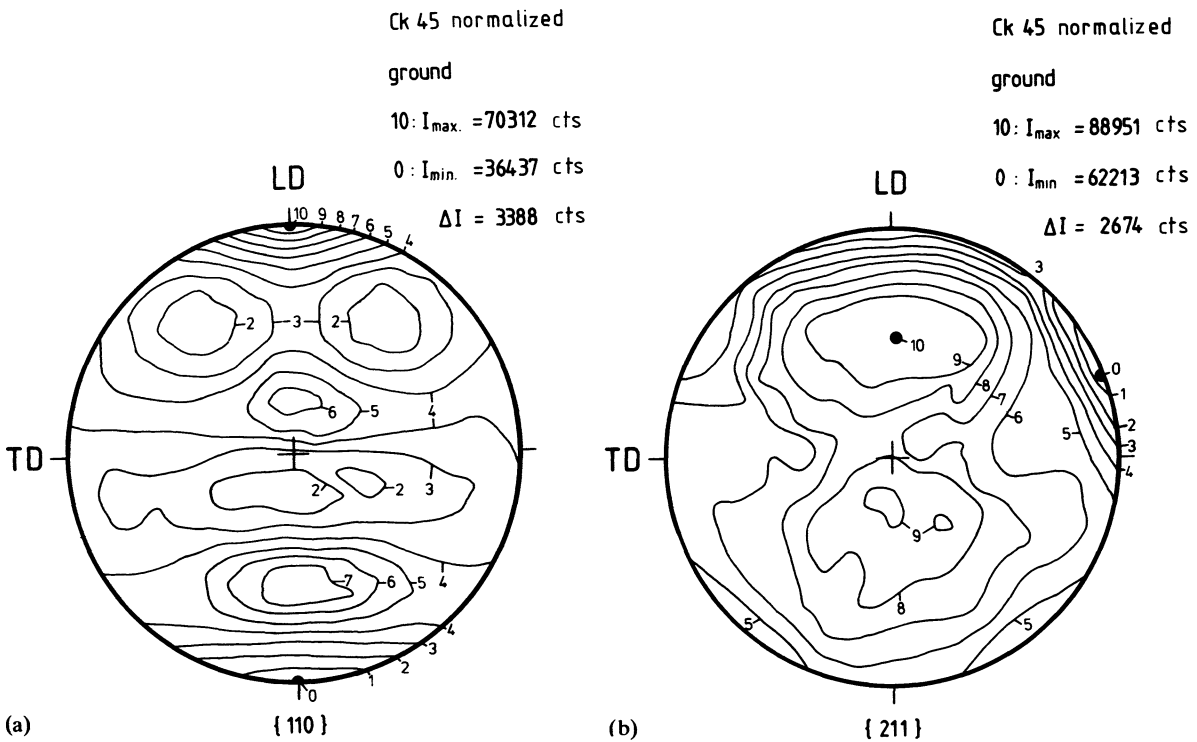

Figure 10 (a) {110}- and (b) {211}-texture pole figures after grinding of a normalized specimen ($0° \leq \psi \leq 70$)

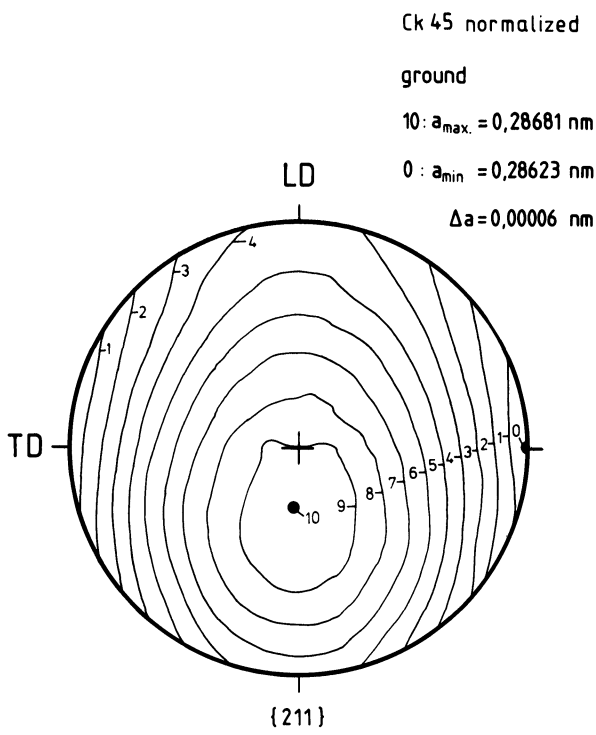

Figure 11 (a) Lattice deformation pole figure measured at {211}-lattice planes after grinding of a normalized specimen ($0° \leq \psi \leq 70°$)

σ_{yy} is much larger than σ_{xx}. τ_{xy} is very small and can be neglected. It is important to note that an average surface normal σ_{zz}-component of considerable magnitude exists within the penetration depth of the X-rays used. By rotating the specimen coordinate system by $-19°$ about TD, the principal stress tensor

$$\Sigma^P = \begin{pmatrix} -273 & 0 & 0 \\ 0 & -438 & 0 \\ 0 & 0 & -85 \end{pmatrix} \text{N/mm}^2 \tag{18}$$

is obtained.

The texture state and the lattice deformation state of cold rolled and ground specimens are shown in Figure 12 and 13. First, a

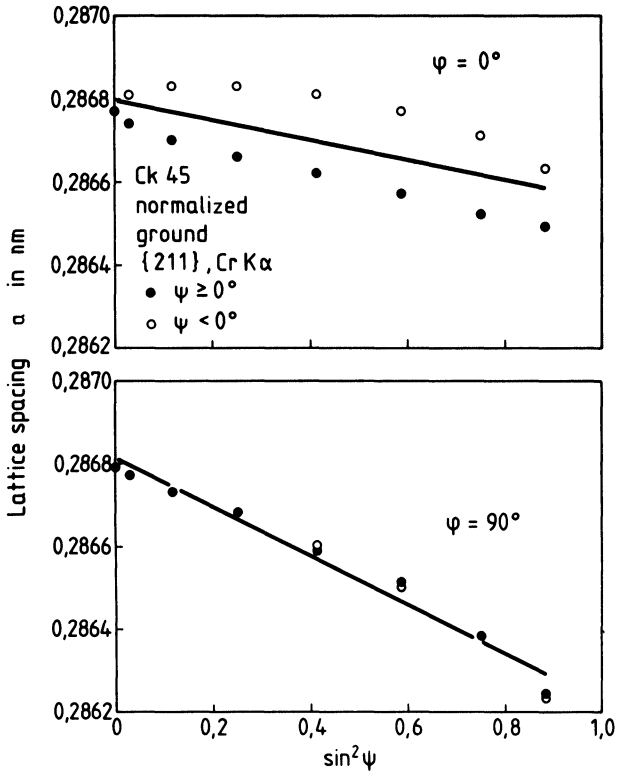

Figure 11 (b) a vs. $\sin^2 \psi$ distribution in the azimuths $\varphi = 0°$ and $\varphi = 90°$ of the pole figure shown in (a)

comparison of Figure 4 and Figure 12 reveals that for both $\{hkl\}$-planes the pole density distributions have been altered by grinding. The differences in the pole densities of the cold rolled state have been smoothed out by the applied machining procedure. The intensity ratios I_{max}/I_{min} are 2.17 and 1.77 for the {110}- and the {211}-pole figure respectively, and are considerably smaller than in the as rolled state. For the {110}- as well as for the {211}-poles a slight tendency for an asymmetry with regard to TD can be stated which is more enhanced in the {110}- than in the {211}-pole figure.

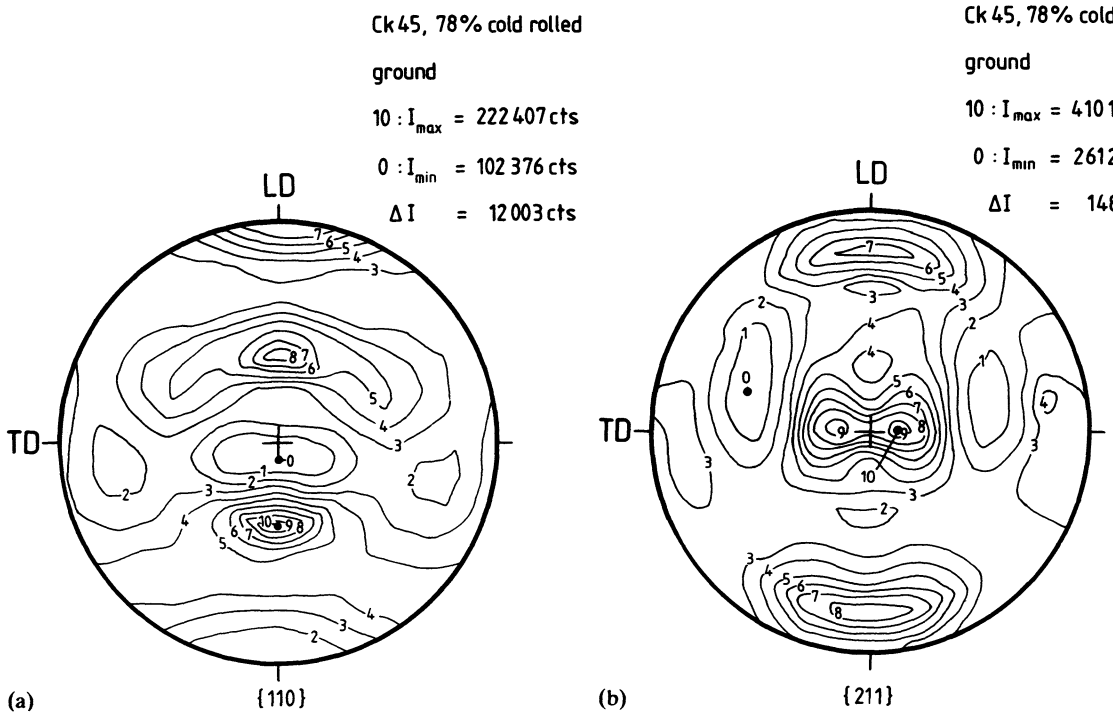

Figure 12 (a) {110}- and (b) {211}-texture pole figures after grinding of a cold rolled specimen ($0° \leq \psi \leq 70°$)

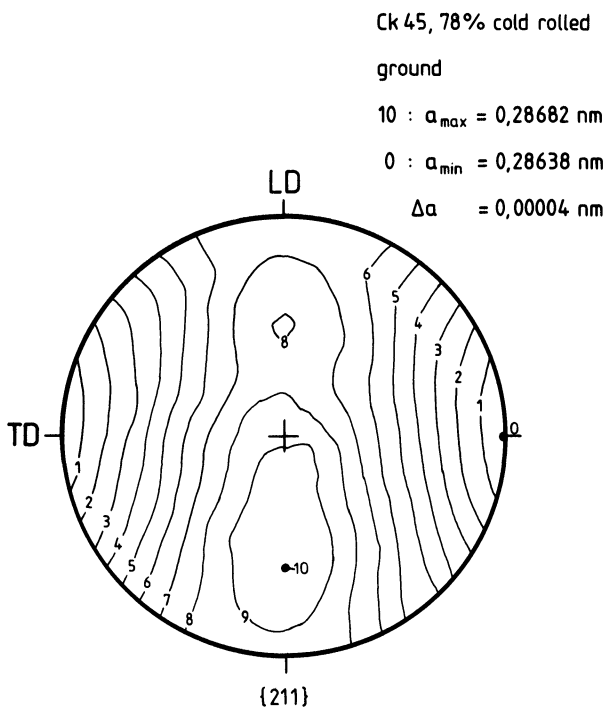

Figure 13 (a) Lattice deformation pole figure measured at {211}-lattice planes after grinding of a cold rolled specimen ($0° \leq \psi \leq 70°$)

Although in both cases the areas of high pole density stayed at nearly the same angular distance to the center of the pole figure, the shape and pole density distributions of these areas change markedly due to the grinding process. For example, in the {110}-pole figure a relative high pole density appeared at $\psi = +70°$ in the azimuth $\varphi = 0°$. The comparison of Figure 13a and Figure 5a reveals that the residual strain state of the 78% cold rolled specimens is severely influenced by a grinding process. This can also be seen from the a vs. $\sin^2 \psi$ distributions in the azimuths $\varphi = 0°$ and $\varphi = 90°$ shown in Figure 13b and Figure 5b. The a-pole figure is symmetrical to TD but quite different from that in a ground normalized specimen (see Figure 11a). The complete residual lattice deformation state, evaluated according to (Wagner *et al.*, 1983) with the X-ray elastic

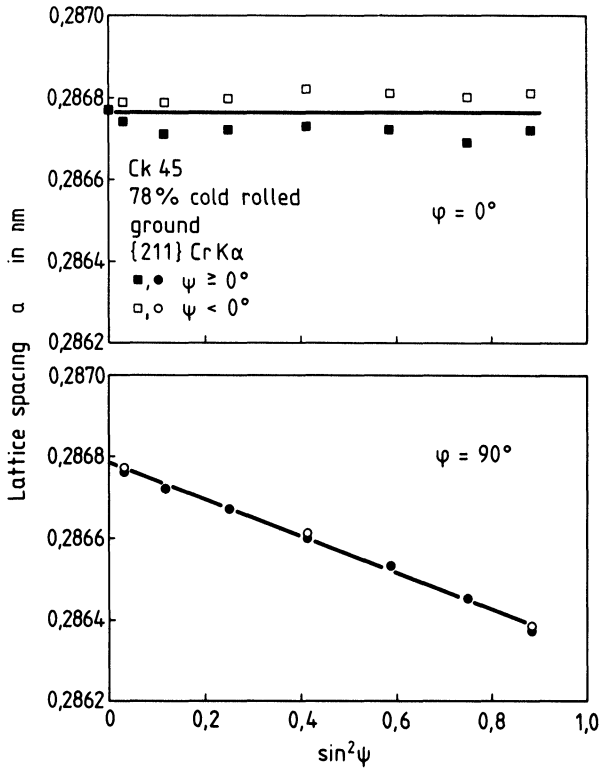

Figure 13 (b) a vs. $\sin^2 \psi$ distribution in the azimuths $\varphi = 0°$ and $\varphi = 90°$ of the pole figure shown in (a)

constants and the value of a_0 given above yields the stress components

$$\Sigma = \begin{pmatrix} 1 & -8 & -32 \\ -8 & -248 & 1 \\ -32 & 1 & 10 \end{pmatrix} \simeq \begin{pmatrix} 0 & 0 & -32 \\ 0 & -248 & 0 \\ -32 & 0 & 0 \end{pmatrix} \text{N/mm}^2 \quad (19)$$

Comparing this with the stress state of the cold rolled specimen (Eq. 11) shows that grinding in this case reduces the magnitude of σ_{xx} to Zero while σ_{yy} is increased. It has to be emphasized that after grinding of the cold-rolled specimen a negligible value of σ_{zz} is observed whereas the stress state after grinding of the normalized

specimen displayed a value of $\sigma_{zz} = -105\,\mathrm{N/mm^2}$. The principal system is obtained by rotating the specimen coordinate system by $-45°$ about TD. The principal stress tensor is

$$\Sigma^P = \begin{pmatrix} -32 & 0 & 0 \\ 0 & -248 & 0 \\ 0 & 0 & +32 \end{pmatrix} \mathrm{N/mm^2} \tag{20}$$

SHOT PEENING OF NORMALIZED AND COLD ROLLED MATERIAL STATES

Shot peening of the normalized specimens leads to the texture pole figures shown in Figure 14. The intensity ratio of the {110}-pole figure is $I_{max}/I_{min} = 1.66$ and of the {211}-pole figure $I_{max}/I_{min} = 1.30$. The {110}-pole figure in Figure 14a shows that {110}-poles preferrably coincide with the normal to the specimen surface. This corresponds with the circular area of high pole density in the {211}-pole figure in an angular distance of $|\psi| = 30°$ to the pole of ND (see Figure 14b).

The residual strain state of the shot peened normalized specimens is shown in Figure 15. The centrosymmetric distribution of the strains is a consequence of the incidence of the shot perpendicular to the specimen surface.

The a-$\sin^2\psi$ distributions in the azimuths $\varphi = 0°$ and $\varphi = 90°$ (Figure 15b) are linear. The residual strain state corresponds to the stress tensor

$$\Sigma = \begin{pmatrix} -425 & 0 & -5 \\ 0 & -423 & 3 \\ -5 & 3 & -40 \end{pmatrix} \simeq \begin{pmatrix} -425 & 0 & 0 \\ 0 & -423 & 0 \\ 0 & 0 & -40 \end{pmatrix} \mathrm{N/mm^2} \tag{21}$$

The stress components in the tensor on the right hand side of Eq. (21) are identical with the principal stresses σ_I, σ_{II} and σ_{III} respectively, and the specimen coordinate system coincides with the principal system.

After shot peening of cold rolled specimens the {110}- and {211}-texture pole figures shown in Figure 16 are found. Compared to Figure 3 it can be seen that the cold rolling texture is not severely

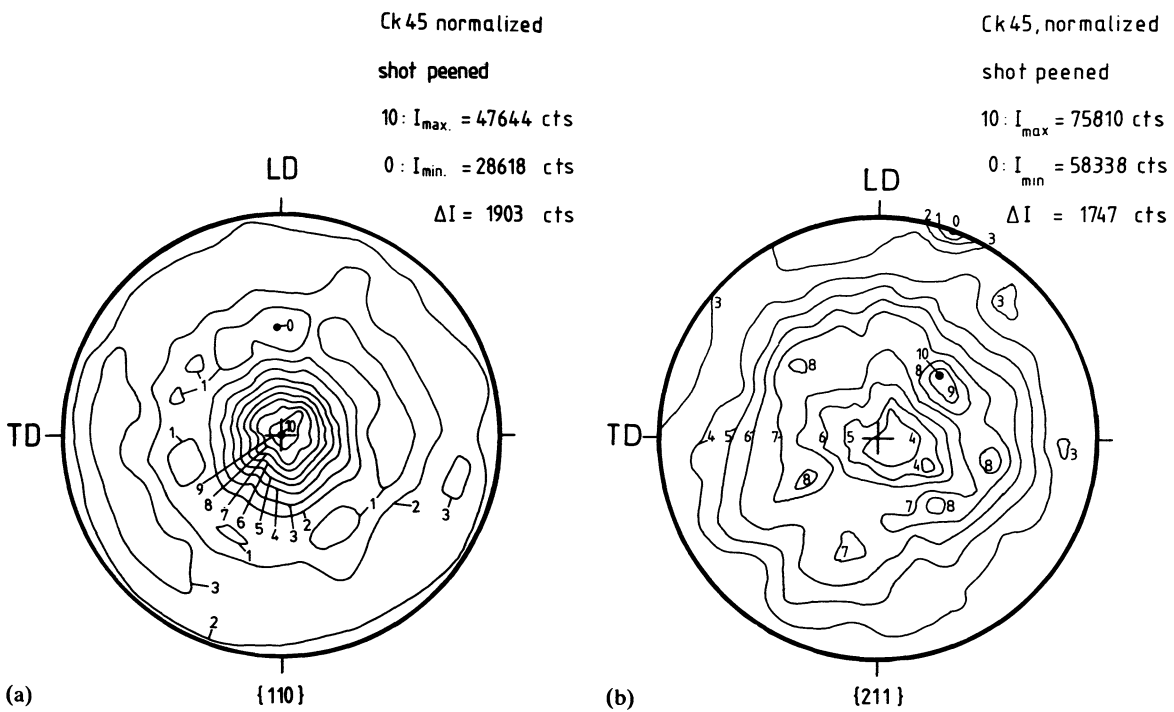

Figure 14 (a) {110}- and (b) {211}-texture pole figures after shot peening of a normalized specimen ($0° \leq \psi \leq 70°$)

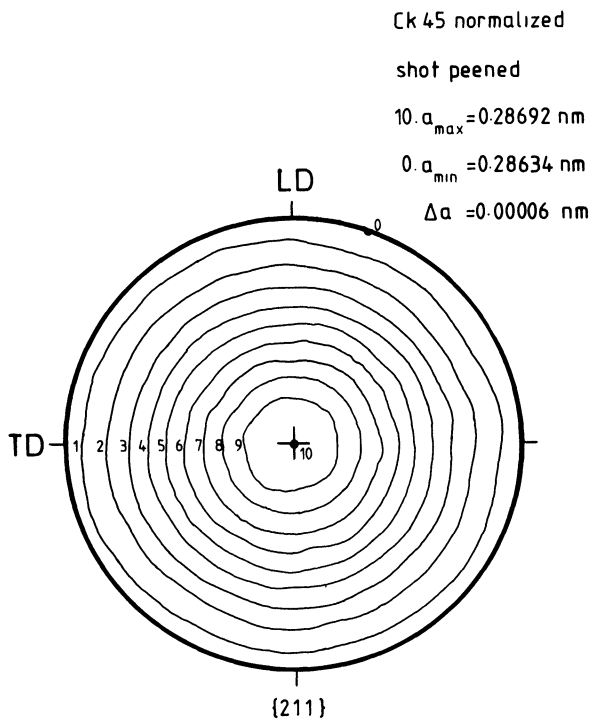

Figure 15 (a) Lattice deformation pole figure measured at {211}-lattice planes after shot peening of a normalized specimen ($0° \leq \psi \leq 70°$)

changed by shot peening. The areas with high pole density observed in the cold rolling texture occur again with similar shape and extension after shot peening. However, shot peening reduces the intensity ratio from the initial value of the {110}-pole figure $I_{max}/I_{min} = 7.47$ to $I_{max}/I_{min} = 3.96$. The initial value of the {211}-pole figure is not significantly changed from $I_{max}/I_{min} = 1.93$ to $I_{max}/I_{min} = 1.91$.

The near surface residual strain state of the cold rolled and subsequent shot peened material is represented by the a-pole figure and the a-$\sin^2\psi$ distributions in the azimuths $\varphi = 0°$ and $\varphi = 90°$ shown in Figure 17. Although there is a marked tendency to attain a

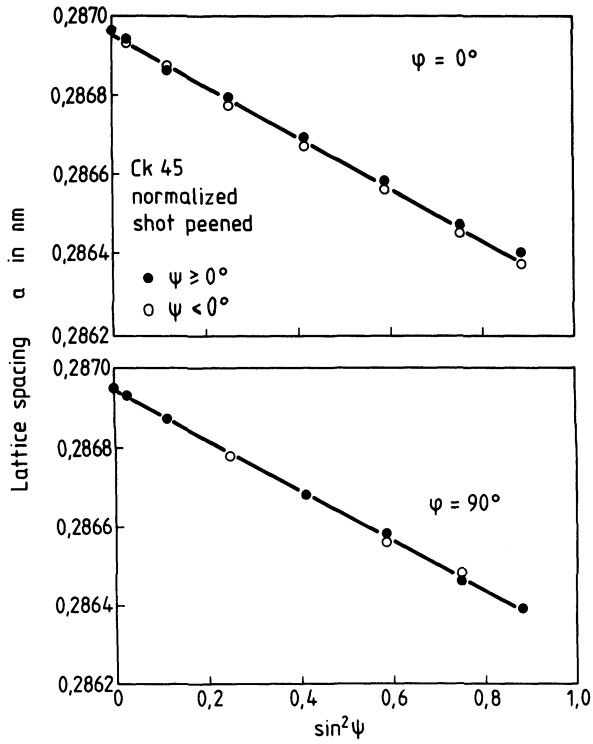

Figure 15 (b) a vs. $\sin^2 \psi$ distributions in the azimuths $\varphi = 0°$ and $\varphi = 90°$ of the pole figure shown in (a)

centrosymmetric lattice deformation state similar to that shown in Figure 15, a comparison with Figure 3a clearly reveals that the strain anomalies due to the cold rolling texture are preserved at least to a small extent. Particularly the a-$\sin^2 \psi$ distribution in the section $\varphi = 0°$ shows that systematic deviations from the regression line fit occur at the same values of $\sin^2 \psi$ as expected from the data shown in Fig. 3b. The residual strain state observed yields the stress state

$$\Sigma = \begin{pmatrix} -458 & 1 & 1 \\ 1 & -468 & 3 \\ 1 & 3 & 7 \end{pmatrix} \approx \begin{pmatrix} -463 & 0 & 0 \\ 0 & -463 & 0 \\ 0 & 0 & 0 \end{pmatrix} \text{N/mm}^2 \quad (22)$$

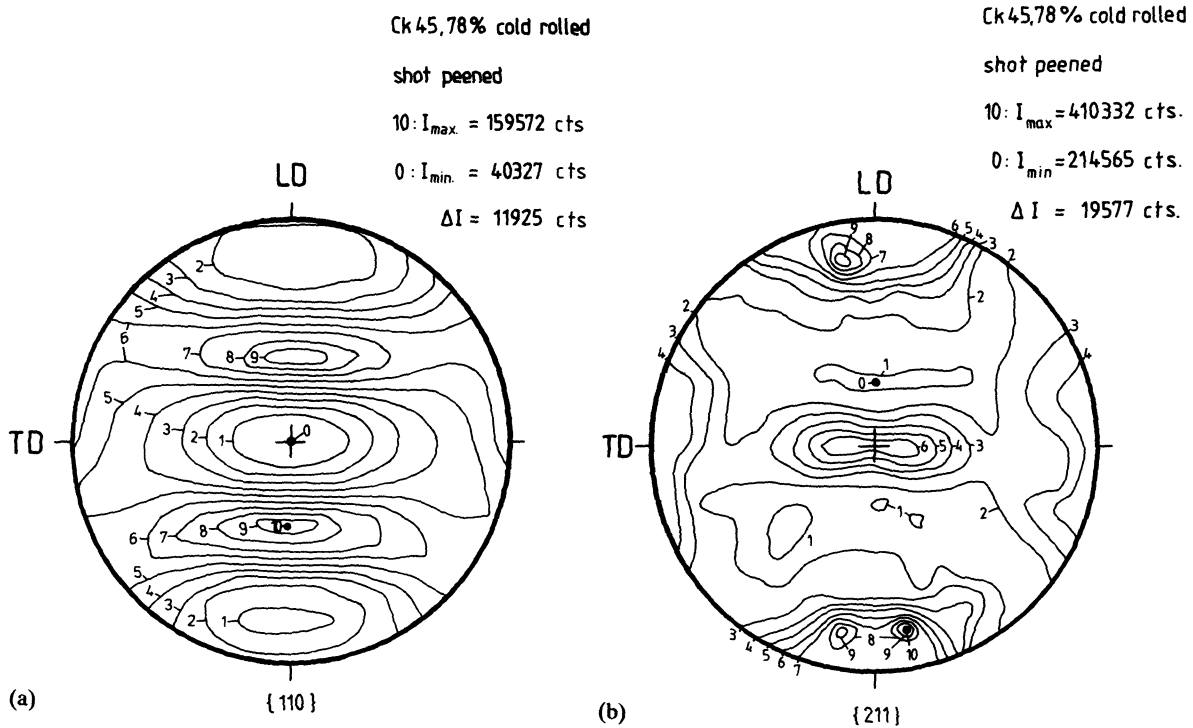

Figure 16 (a) {110}- and (b) {211}-texture pole figures after shot peening of a cold rolled specimen ($0° \leq \psi \leq 70°$)

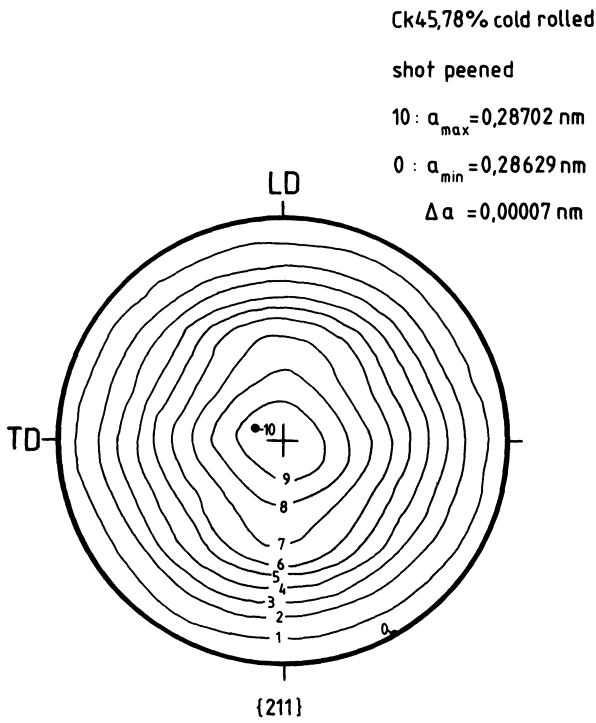

Figure 17 (a) Lattice deformation pole figure measured at {211}-lattice planes after shot peening of a cold rolled specimen ($0° \leq \psi \leq 70°$)

This shows that the shot peening induced plastic deformation in the surface layer produce, as is also the case in the normalized material, a residual strain state, which is well described by a biaxial surface parallel principal stress state. However, the magnitude of the principal stresses are larger than in the normalized material. Furthermore, after shot peening of cold rolled specimens, no significant surface normal stress component σ_{zz} like in the normalized shot peened specimen was found.

CONCLUSIVE REMARKS

The experimental results presented show that compared to the starting condition the grain orientation distributions in the mach-

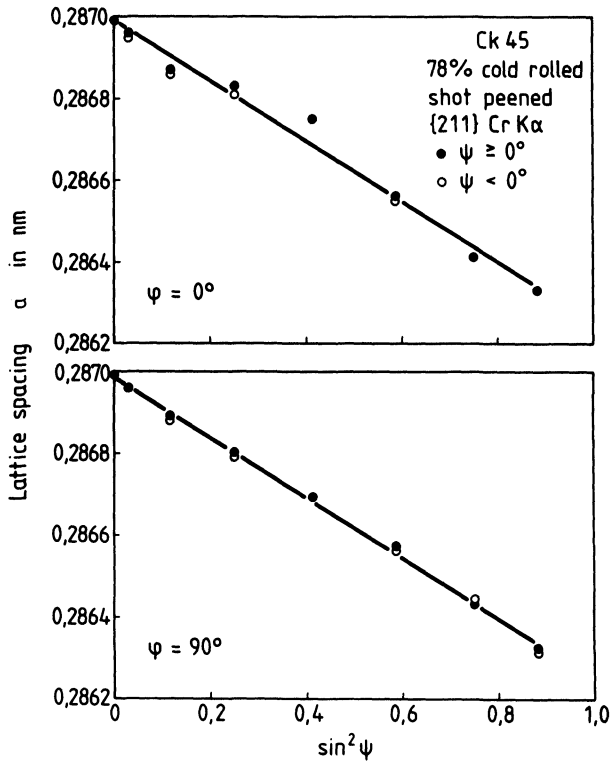

Figure 17 (b) a vs. $\sin^2 \psi$ distributions in the azimuth $\varphi = 0°$ and $\varphi = 90°$ of the pole figure shown in (a)

ined surface of differently pretreated plain carbon steel are markedly changed by milling, grinding, and shot peening. In specimens that are initially texture free, typical machining textures develop due to the individual operations applied. In cold rolled specimens the rolling textures are superposed with the machining textures. The strength of the rolling texture is diminished by machining and extensive changes of the pole density distributions are produced. In the case of shot peening, the deforming forces mainly act perpendicular to the surface and tend to generate a fibre-like texture with an {110}-fibre axis parallel to the normal of the shot peened surface, and a residual stress state with $\sigma_{xx} \simeq \sigma_{yy} \simeq \sigma_I \simeq \sigma_{II}$. Independent of the original state the final textures after milling and grinding are asymmetric, mainly with regard to the TD-axis of the

specimen system. Asymmetries are also found in the appertaining residual lattice strain distributions. The ψ-splitting observed may be caused by shear stress components. If the measured residual lattice strain distributions are evaluated according to Eq. (1), values of σ_{zz}, τ_{xz} and τ_{yz} can be calculated. However, it follows from the equilibrium conditions of the linear theory of elasticity that all surface normal stress components σ_{zz}, τ_{xz} and τ_{yz}, as well as their gradients $d\sigma_{zz}/dz$, $d\tau_{xz}/dz$ and $d\tau_{yz}/dz$ vanish at the specimen surface. Hence only surface parallel stress components are allowed in the specimen surface. With the assumption of a biaxial, surface parallel stress state, (Brakman, 1983, van Baal, 1983) theoretically predicted ψ-splitting as a consequence of asymmetric textures which lead to distinct elastic constants in particular ψ-directions and appertaining residual lattice strains.

However, the specimens investigated in experiments presented in this paper showed ψ-splitting also after electrolytically removing the surface layers with the asymmetric textures. Obviously, in these cases texture effects cannot be solely responsible for the observed ψ-splitting. On the other hand it can be concluded that despite of the equilibrium conditions of the linear theory of elasticity (Krause and Öcalan, 1984, Dölle and Cohen 1980) the observed shear stresses τ_{xz} and τ_{yz} are micro-residual stresses which may occur in materials with heterogeneous microstructures where their compensation is possible on a microscopic scale. Furthermore, it has to be taken into consideration that the residual strain informations sampled by the X-rays are weighted averages over a certain penetration depth where the existence of stress components σ_{zz}, τ_{xz} and τ_{yz} cannot completely be excluded.

The values of σ_{zz} observed in these experiments depend on the pretreatment of the specimens. While in the normalized specimens after milling, grinding, or shot peening always negative values of σ_{zz} were determined with respect to the cited value of a_0, the values of σ_{zz} were negligible after grinding or shot peening of cold rolled specimens. But a negative value of σ_{zz} was also found after milling of a cold rolled specimen.

The experimental results presented allow to state that the applied machining operations produce typical texture states and residual stress states. Machining residual stresses have for a long time been measured and taken into consideration in the design and production

of structural parts while the machining induced textures were mostly ignored. However, there are quite a number of physical properties, e.g. the materials response to fatigue loading, friction and corrosion, that are also sensitive to the grain orientation in the loaded specimen surface. In order to improve the life time of parts under texture sensitive loading states it is necessary to monitor and, if possible, manipulate the texture state of the specimen surface in the desired way. Thus it is proposed that machining textures are taken into considerations in addition to the characteristic physical properties that have already been in use for the assessment of the material state in machined surfaces.

Acknowledgement

The research presented in this paper was funded by the Bundesministerium für Forschung und Technologie under Grant-No. 523-4001-01 ZG 1425. Responsibility for the publication lies with the authors.

References

Baal, C. M. van (1983). *Phys. Stat. Sol.* (a) **77,** 521–526.
Brakman, C. M. (1983). *J. Appl. Cryst.* **16,** 325–340.
Bechmann, R. and Hearmon, R. F. S. (1966). *Landolt-Börnstein: Zahlenwerte und Funktionen, Gruppe III,* Bd. 1, edited by K.-H. Hellwege and A. M. Hellwege, Springer-Verlag, Berlin, Heidelberg, New York.
Christian, H. (1971). *Härterei-Tech. Mitt.* **26,** 180–198.
Dölle, H. and Cohen, J. B. (1980). *Met. Transactions* A **11,** 159–164.
Dölle, H. and Hauk, V. (1976). *Härterei-Tech. Mitt.* **31,** 165–168.
Fritsche, G., Kämpfe, B. and Zimmermann, P. (1979). *Die Technik* **34,** 611–614.
Hauk, V., Heil, W. and Stuitje, P. J. T. (1985). *Z. Metallkde.* **76,** 640–648.
Hauk, V., Krug, W. K., Vaessen, G. J. H. and Weisshaupt, H. (1980). *Härterei-Tech. Mitt.* **35,** 144–147.
Hauk, V. and Stuitje, P. J. T. (1983). *Eigenspannungen,* edited by E. Macherauch and V. Hauk, DGM Informationsgesellschaft Verlag, Oberursel, Bd.2, 271–285.
Hauk, V. and Vaessen, G. (1983). *Eigenspannungen und Lastspannungen,* edited by V. Hauk and E. Macherauch, Carl Hanser Verlag, München, Wien, 38–48.
Hauk, V., Vaessen, G. J. H. and Weber, B. (1985). *Härterei-Tech. Mitt.* **40,** 122–128.
Hoffmann, J. (1985). Dr.-Ing. thesis, Universität Karlsruhe.
Hoffmann, J. Maurer, G., Neff, H., Scholtes, B. and Macherauch, E. (1985). *Experimental methods of texture analysis,* DGM Informationsgesellschaft Verlag, Oberursel, 409–418.
Hoffmann, J., Neff, H., Scholtes, B. and Macherauch, E. (1983). *Härterei-Tech. Mitt.* **38,** 180–183.
Krause, H. and Mathias, J. (1983). *Härterei-Tech. Mitt.* **38,** 129–135.
Krause, H. and Öcalan E. (1984). Proceedings of the seventh international

conference on textures of materials, edited by C. M. Brakman, P. Jongenburger, E. J. Mittemeijer 625–630.
Macherauch, E. *et al.* (1987). In *Residual Stresses in Science and Technology*, edited by E. Macherauch and V. Hauk, DGM Informationsgesellschaft Verlag, Oberursel.
Macherauch, E. and Müller, P. (1961). *Z. angew. Physik* **13,** 305–312.
Maurer, G., Neff, H., Scholtes, B. and Macherauch, E. (1987). *Z. Metallkde.* **78,** 1–7.
Reuss, A. (1929). *Z. angew. Mathematik und Mechanik* **9,** 49–58.
Savchuck, V. I., Moroz, I. A., Ivaniji, V. S. and Grishkevich, A. S. (1979). *Kristall und Technik* **14,** 471–474.
Voigt, W. (1928). *Lehrbuch der Kristallphysik,* Teubner-Verlag, Berlin, Leipzig, 1. ed.
Wagner, C. N. J., Boldrick, M. S. and Perez-Mendex, V. (1983). *Adv. in X-ray Analysis* **26,** 275–282.
Wassermann, G. and Grewen, J. (1962). *Texturen metallischer Werkstoffe,* Springer-Verlag, Berlin, Heidelberg, New York.
Wolfstieg, U. and Macherauch, E. (1976). *Härterei-Tech. Mitt.* **31,** 83–85.